Phonon renormalization in doped bilayer graphene

A. Das,[1] B. Chakraborty,[1] S. Piscanec,[2] S. Pisana,[2] A. K. Sood,[1,*] and A. C. Ferrari[2,†]
[1]*Department of Physics, Indian Institute of Science, Bangalore 560012, India*
[2]*Department of Engineering, Cambridge University, Cambridge CB3 0FA, United Kingdom*
(Received 10 July 2008; published 13 April 2009)

We report phonon renormalization in bilayer graphene as a function of doping. The Raman *G* peak stiffens and sharpens for both electron and hole doping as a result of the nonadiabatic Kohn anomaly at the Γ point. The bilayer has two conduction and valence subbands, with splitting dependent on the interlayer coupling. This gives a change of slope in the variation of *G* peak position with doping which allows a direct measurement of the interlayer coupling strength.

DOI: 10.1103/PhysRevB.79.155417 PACS number(s): 73.63.−b

I. INTRODUCTION

Graphene is the latest carbon allotrope to be discovered.[1–5] Near-ballistic transport at room temperature and high carrier mobilities[2–8] make it a potential material for nanoelectronics,[9–11] especially for high-frequency applications. It is now possible to produce areas exceeding thousands of square microns by means of micromechanical cleavage of graphite. An ongoing effort is being devoted to large scale deposition and growth on different substrates of choice.

Unlike single layer graphene (SLG), where electrons disperse linearly as massless Dirac fermions,[1–5] bilayer graphene (BLG) has two conduction and valence bands, separated by γ_1, the interlayer coupling.[12,13] This was measured to be ~0.4 eV by angle-resolved photoelectron spectroscopy[14] and ~0.43 eV by cyclotron resonance experiment.[15] A gap between valence and conduction bands could be opened and tuned by an external electric field,[16,17] making BLG a tunable-gap semiconductor.

Graphene can be identified in terms of number and orientation of layers by means of inelastic and elastic light scatterings, such as Raman[18] and Rayleigh spectroscopies.[19,20] Raman spectroscopy also allows monitoring of doping, defects, edges, strain, and chemical modifications.[4,21–31] Indeed, Raman spectroscopy is a fast and nondestructive characterization method for carbons.[32] They show common features in the 800–2000 cm^{-1} region: the *G* and *D* peaks, around 1580 and 1350 cm^{-1}, respectively. The *G* peak corresponds to the E_{2g} phonon at the Brillouin-zone center (Γ). The *D* peak is due to the breathing modes of sp^2 atoms and requires a defect for its activation.[33–35] The most prominent feature in SLG is the second order of the *D* peak: the 2*D* peak.[18] This lies at ~2690 cm^{-1} and involves phonons at $\mathbf{K}+\Delta\mathbf{q}$.[18,24] $\Delta\mathbf{q}$ depends on the excitation energy, due to double resonance, and the linear dispersion of the phonons around $\mathbf{K}$.[18,35,36] 2*D* is a single peak in SLG, whereas it splits in four in BLG, reflecting the evolution of the band structure.[18] The 2*D* peak is always seen, even when no *D* peak is present, since no defects are required for overtone activation.

In SLG, the effects of back and top gatings on *G*-peak position [Pos(*G*)] and full width at half maximum [FWHM(*G*)] were reported in Refs 21, 22, and 25. Pos(*G*) increases and FWHM(*G*) decreases for both electron and hole doping. The *G* peak stiffening is due to the nonadiabatic removal of the Kohn anomaly at Γ.[21,37] FWHM(*G*) sharpening is due to blockage of phonon decay into electron-hole pairs due to the Pauli exclusion principle, when the electron-hole gap is higher than the phonon energy,[21,38] and saturates for a Fermi shift bigger than half phonon energy.[21,22,38] A similar behavior is observed for the *LO*-G^- peak in metallic nanotubes[39] for the same reasons. The conceptually different BLG band structure is expected to renormalize the phonon response to doping differently from SLG.[13,40] Here we prove this by investigating the effect of doping on the BLG *G* and 2*D* peaks. The *G* peak of doped BLG was recently investigated,[41,42] but reproduced that of SLG we previously measured,[21,25] due to the very low doping range (~5 $\times 10^{12}$ cm^{-2}), not enough to cross the second BLG subband. Here we reach much higher values (~5×10^{13} cm^{-2}), probing the further renormalization resulting from crossing to the second BLG subband.

II. BILAYER GRAPHENE

The lattice structure of bilayer graphene is shown in Fig. 1(a), where the bottom and top layers are represented by a dashed red line and solid blue line, respectively. The indexes 1 and 2 in Fig. 1(a) label the sublattices of the bottom and top layers, respectively.[43–46] As seen from Fig. 1(a), the A_2

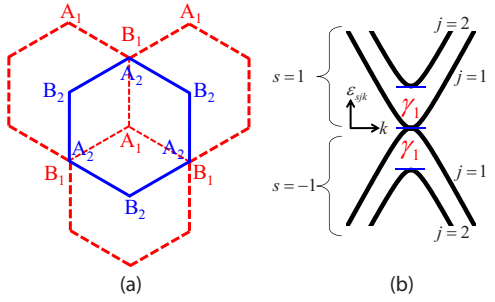

FIG. 1. (Color online) (a) Top view of a bilayer graphene. Red dotted line represents the bottom layer, while the solid blue line the top layer. A_1 and B_1 are the sublattices of the bottom layer, and A_2 and B_2 those of the top layer. (b) Energy dispersion of a bilayer graphene. γ_1 is the energy separation between the two subbands. $s=+1$ for conduction band and $s=-1$ for valence band.

sublattice of the top layer is exactly on top of the sublattice B_1 of the bottom layer. In the tight-binding approximation, the in-plane nearest-neighbor hopping energy (A_1-B_1 or A_2-B_2) is called γ_0, whereas the interlayer hopping energy (A_2-B_1) is γ_1. These are the most relevant energy scales of a bilayer graphene. Here, we neglect in-plane next-nearest-neighbor hopping and interlayer second-nearest-neighbor hopping γ_3 (B_2-A_1) and γ_4 (A_2-A_1 or B_2-B_1). Under these approximations, the Hamiltonian of a bilayer graphene near the **K** point can be written as[43–46]

$$\mathbf{H} = \begin{pmatrix} 0 & \gamma\mathbf{k} & 0 & 0 \\ \gamma\mathbf{k} & 0 & \gamma_1 & 0 \\ 0 & \gamma_1 & 0 & \gamma\mathbf{k} \\ 0 & 0 & \gamma\mathbf{k} & 0 \end{pmatrix}, \tag{1}$$

where $\gamma = \frac{\sqrt{3}}{2}\gamma_0 a$ and a is the lattice parameter. The eigenvalues of this Hamiltonian are

$$\epsilon_{sj}(k) = s\left[\left(\sqrt{\left(\frac{\gamma_1}{2}\right)^2 + (\gamma_0 k)^2}\right)(-1)^j \frac{\gamma_1}{2}\right], \tag{2}$$

where s is a band index: +1 for conduction band and −1 for valence band. j is the subband index, whose values are 1 and 2, as shown in Fig. 1(b). This also plots the energy dispersion of a bilayer graphene, where γ_1 (Refs. 12, 13, and 43–46) measures the energy separation between the two subbands. The density of states (DOS) is calculated using Eq. (2) and is given by

$$D(\epsilon) = \frac{4}{2\pi\gamma^2}\left(\epsilon + \frac{\gamma_1}{2}\right), \quad \text{for } \epsilon < \gamma_1$$

$$D(\epsilon) = \frac{8\epsilon}{2\pi\gamma^2}, \quad \text{for } \epsilon > \gamma_1. \tag{3}$$

In comparison, single layer graphene has linear energy dispersion $\epsilon_s(k) = s[\gamma k]$ and $D(\epsilon) = \frac{4\epsilon}{2\pi\gamma^2}$.

III. EXPERIMENTAL

A. Electrochemical top gating

We recently demonstrated a SLG top gated by polymer electrolyte[25] able to span a large doping range—up to $\sim 5 \times 10^{13}$ cm^{-2}. This is possible because the nanometer-thick Debye layer[25,47,48] gives a much higher gate capacitance compared to the usual 300 nm SiO_2 back gate.[5] We apply here this approach to BLG. Figure 2 shows the scheme of our experiment. A sample is produced by micromechanical cleavage of graphite. This consists of a SLG extending to a BLG, as proven by the characteristic SLG and BLG 2*D* peaks in the inset of Fig. 2.[18] An Au electrode is then deposited by photolithography covering both SLG and BLG (Fig. 2). Top gating is achieved by using a solid polymer electrolyte[25] consisting of $LiClO_4$ and polyethylene oxide (PEO) in the ratio 0.12:1. The gate voltage is applied by placing a platinum electrode in the polymer layer. Note that the particular shape of our sample, consisting of a BLG, with a protruding SLG, ensures the top gate to be effectively applied to both layers. Measurements are done with a WITEC confocal (X50 objective) spectrometer with 600 lines/mm grating, 514.5 nm excitation, and at <1 mW to avoid heating. For a given top gate voltage, V_{TG}, spectra are recorded after 10 min. Figures 3(a) and 3(b) plot the spectra as a function of V_{TG}. We use Voigt functions to fit the *G* peak in both SLG and BLG. The SLG 2*D* band is fitted to one Lorentzian. The BLG 2*D* band is fitted to four Lorentzians $2D_{1A}$, $2D_{1B}$, $2D_{2A}$, and $2D_{2B}$ as in Ref. 18 (Fig. 2). As previously discussed, two of these, $2D_{1A}$ and $2D_{2A}$, are much stronger.[18] Thus, we focus on these. We just note that the relative positions of the four subbands could slightly change with gating if the relative position of the subbands is modified.

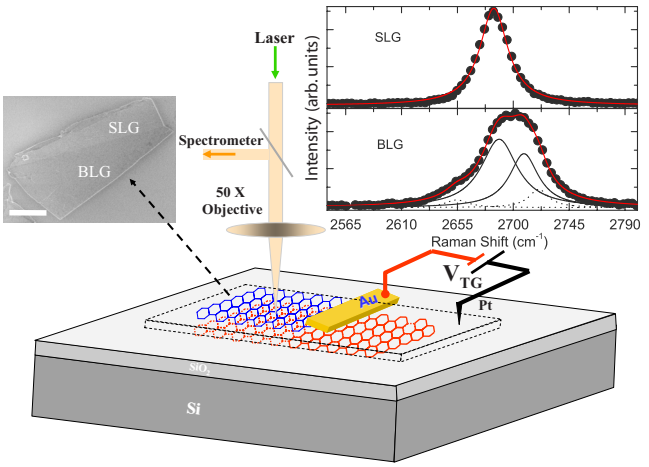

FIG. 2. (Color online) Experimental setup. The black dotted box on SiO_2 indicates the polymer electrolyte (PEO+$LiClO_4$). Left inset shows a scanning electron microscope image of the SLG and BLG. Scale bar: 4 μm. Right inset, comparison of the 2*D* Raman band for our SLG and BLG.

B. Conversion of gate voltage into Fermi-level shift

To get a quantitative understanding, it is necessary to convert V_{TG} into a Fermi level (E_F) shift. In general, the application of a gate voltage (V_G) creates an electrostatic potential difference ϕ between the graphene and the gate electrode and a E_F shift as a result of addition of charge carriers. Therefore, $V_G = \frac{E_F}{e} + \phi$, where ϕ and E_F/e are determined by the geometrical capacitance (C_G) and the quantum capacitance (C_Q) of graphene, respectively. The two capacitors are in series, as in Fig. 4(a). Figure 4(b) depicts schematically the electrostatic voltage drops in our top gated experiment containing both SLG and BLG.

In a top gate experiment V_{TG} is applied between the gate and source. Note that in electrochemical top gating, the voltage drops across the Debye layer, while the voltage drops across the SiO_2 interface in case of back gating. Φ^{SLG} is the electrostatic voltage drop between the Debye layer and the SLG surface. Similarly, Φ^{BLG} is the voltage drop between the Debye layer and the BLG surface. For a bilayer there will be another voltage drop (δV) between the two carbon layers due to the external electric field created by the gate electrode.

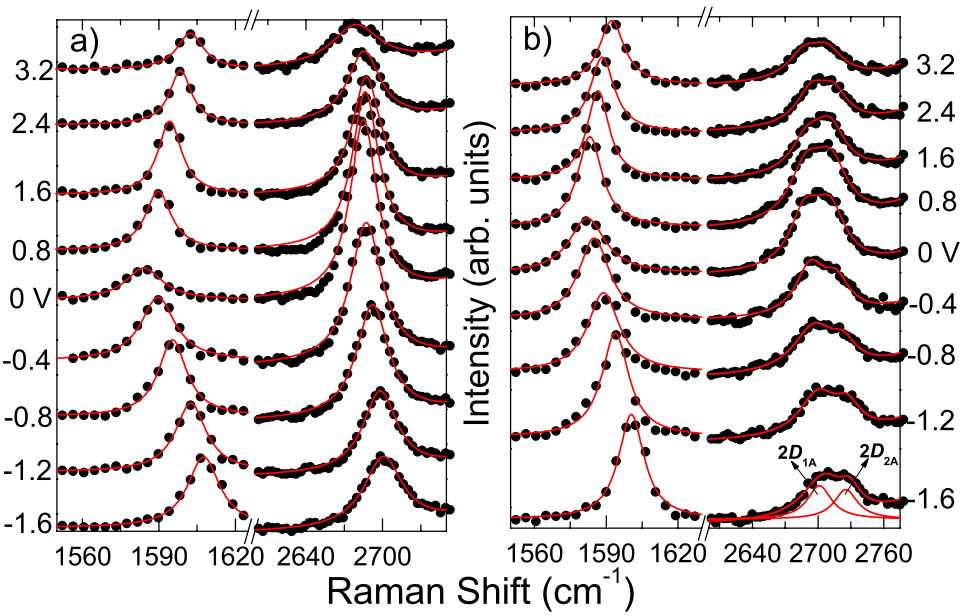

FIG. 3. (Color online) Raman spectra of (a) SLG; (b) BLG at several V_{TG}. Lines are the fits to the experimental data.

Here, we assume equal charge density in both layers. Thus, the total electrostatic voltage drop in BLG is $\Phi_T^{BLG}=\Phi^{BLG}+\delta V$. δV would move the relative position of the conduction and valence band in BLG.[17] In our experimental geometry (Fig. 2) once the equilibrium is reached, both SLG and BLG will have the same chemical potential. Therefore, $eV_{TG}=e\Phi^{SLG}+E_F^{SLG}=e\Phi_T^{BLG}+E_F^{BLG}$, where E_F^{SLG} and E_F^{BLG} are the Fermi energy shifts in SLG and BLG, respectively. In our calculation we neglect the term δV, since, for a given charge density, the value of δV is always smaller compared to E_F^{BLG} and Φ^{BLG}.[16,17,49] Thus

$$eV_{TG}=e\Phi^{SLG}+E_F^{SLG}\cong e\Phi^{BLG}+E_F^{BLG}. \quad (4)$$

The electrostatic potential $\phi=\frac{ne}{C_{TG}}$, where n is the carrier concentration and is calculated using the relation $n=\int_0^{\epsilon_F}D(\epsilon)d\epsilon$. For SLG, $n^{SLG}=\mu E_F^2$, where $\mu=\frac{g_s g_v}{4\pi\gamma^2}=\frac{1}{\pi(\hbar v_F)^2}$, $g_s=g_v=2$ are spin and valley degeneracies, and v_F is the Fermi velocity. Thus for SLG

$$eV_{TG}=\nu E_F^2+E_F. \quad (5)$$

Similarly, for BLG[13,50,51]

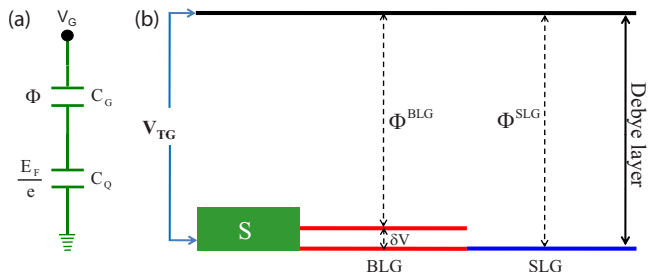

FIG. 4. (Color online) (a) Geometrical capacitance and quantum capacitance are in series with V_G. (b) V_{TG} is the voltage applied between the gate and source. Φ is the electrostatic potential drop and E_F is the Fermi energy shift. δV is the voltage drop between the BLG layers.

$$n^{BLG}=\mu(\gamma_1 E_F+E_F^2), \quad \text{for } E_F<\gamma_1,$$

$$n^{BLG}=2\mu E_F^2, \quad \text{for } E_F>\gamma_1. \quad (6)$$

Thus for BLG

$$eV_{TG}=\nu E_F^2+(1+\nu\gamma_1)E_F, \quad \text{for } E_F<\gamma_1,$$

$$eV_{TG}=2\nu E_F^2+E_F, \quad \text{for } E_F>\gamma_1, \quad (7)$$

where $\nu=\frac{e^2}{\pi C_{TG}(\hbar v_F)^2}$. We take[39] $C_{TG}=2.2\times10^{-6}$ F cm^{-2} and $\gamma_1=0.39$ eV constant with doping [since its variation for n up to $\sim10^{13}$ cm^{-2} is $<5\%$ (Refs. 14 and 16)]. Using Eqs. (5) and (7) we plot the Fermi energy shift for SLG and BLG as a function of gate voltage in Fig. 5.

IV. RESULTS

The dotted lines in Fig. 6 are the experimental Pos(G), FWHM(G) as a function of E_F. In SLG, Pos(G) does not increase up to $E_F\sim0.1$ eV ($\sim\hbar\omega_0/2$), where ω_0 is the frequency of the E_{2g} phonon in the undoped case [$\hbar\omega_0/(2\pi\hbar c)=$Pos($G_0$), with c the speed of light], and then

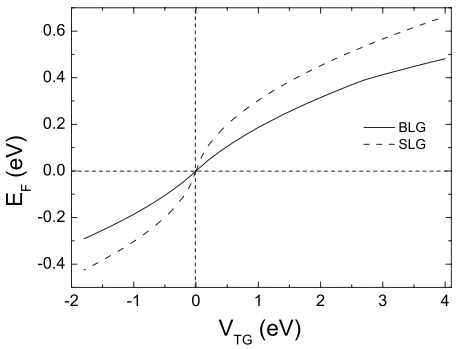

FIG. 5. Fermi energy shift as a function of V_{TG}. Dashed line: SLG; solid line: BLG.

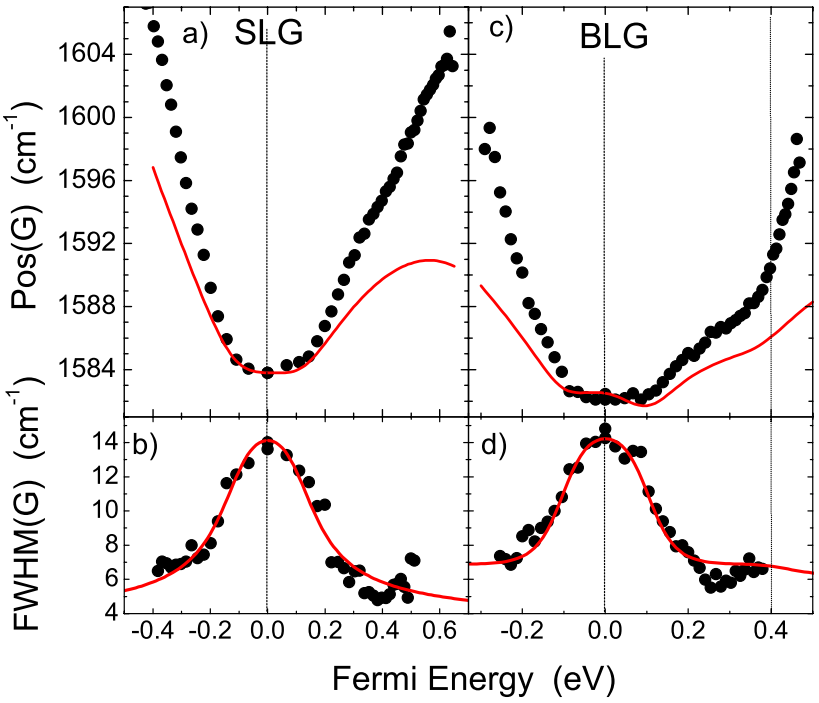

FIG. 6. (Color online) Pos(G) for (a) SLG; (c) BLG as a function of Fermi energy. FWHM(G) of (b) SLG; (d) BLG as a function of Fermi energy. Solid lines: theoretical predictions.

increases with E_F. Figures 6(b) and 6(d) indicate that in SLG and BLG, FWHM(G) decreases for both electron and hole doping, as expected[21] since phonons decay into real electron-hole pairs when $E_F < \hbar\omega_0/2$. Figure 6(c) plots Pos(G) of BLG. We find that (i) Pos(G) does not increase until $E_F \sim 0.1$ eV ($\sim\hbar\omega_0/2$). (ii) Between 0.1 and 0.4 eV the BLG slope $R = \frac{d\mathrm{Pos}(G)}{dE_F}$ is smaller than the SLG one. (iii) A kink is observed in Fig. 6(c) at $E_F \sim 0.4$ eV. (iv) For $E_F > 0.4$ eV the slope is larger than in SLG. (v) The kink position does not significantly depend on γ_1 used to convert V_{TG} in E_F (e.g., ~66% change in γ_1 modifies E_F by ~6%).

V. DISCUSSION

These trends can be explained by considering the effects of doping on the phonons: (i) a change of the equilibrium lattice parameter with a consequent "static" stiffening/softening, $\Delta\mathrm{Pos}(G)^{\mathrm{st}}$; (ii) the onset of "dynamic" effects[21,37] beyond the adiabatic Born-Oppenheimer approximation that modify the phonon dispersion close to the Kohn anomalies, $\Delta\mathrm{Pos}(G)^{\mathrm{dyn}}$. Thus, the total phonon renormalization can be written as[21,37]

$$\mathrm{Pos}(G_{E_F}) - \mathrm{Pos}(G_0) = \Delta\mathrm{Pos}(G) = \Delta\mathrm{Pos}(G)^{\mathrm{st}} + \Delta\mathrm{Pos}(G)^{\mathrm{dyn}}. \tag{8}$$

For SLG, we get $\Delta\mathrm{Pos}(G)^{\mathrm{st}}$ by converting E_F into the corresponding electron density n^{SLG} and[37,52]

$$\Delta\mathrm{Pos}(G)^{\mathrm{st}} = -2.13n - 0.0360n^2 - 0.00329n^3 - 0.226|n|^{3/2}, \tag{9}$$

where n, in units of 10^{13} cm^{-2}, is positive and negative for electron and hole doping, respectively. For BLG, we assume n^{BLG} equally distributed on the two layers, each behaving as a SLG with an electron concentration $n^{\mathrm{BLG}}/2$, and use the above relation to compute $\Delta\mathrm{Pos}(G)^{\mathrm{st}}$.

$\Delta\mathrm{Pos}(G)^{\mathrm{dyn}}$ is calculated from the phonon self-energy[53] Π,

$$\hbar\Delta\mathrm{Pos}(G)^{\mathrm{dyn}} = \mathrm{Re}[\Pi(E_F) - \Pi(E_F = 0)]. \tag{10}$$

The electron-phonon coupling (EPC) contribution to FWHM(G) is given by[53–55]

$$\mathrm{FWHM}(G)^{\mathrm{EPC}} = 2\,\mathrm{Im}[\Pi(E_F)]. \tag{11}$$

The self-energy for the E_{2g} mode at Γ in SLG can be written as[21,37,57]

$$\Pi(E_F)^{\mathrm{SLG}} = \alpha' \int_{-\infty}^{\infty} \frac{f(\epsilon) - f(-\epsilon)}{2\epsilon + \hbar\omega_0 + i\delta} |\epsilon| d\epsilon, \tag{12}$$

while for BLG it is given by[13]

$$\Pi(E_F)^{\mathrm{BLG}} = \alpha' \int_0^{\infty} \gamma^2 k dk \sum_{s,s'} \sum_{j,j'} \phi_{jj'}^{+} \times \frac{[f(\epsilon_{sjk}) - f(\epsilon_{s'j'k})][\epsilon_{sjk} - \epsilon_{s'j'k}]}{(\epsilon_{sjk} - \epsilon_{s'j'k})^2 - (\hbar\omega + i\delta)^2}, \tag{13}$$

where $\alpha' = \frac{\hbar A_{uc}\mathrm{EPC}(\Gamma)^2}{\pi M\omega_0(\hbar v_F)^2}$, $A_{\mathrm{uc}} = 5.24$ Å^2 is the graphene unit-cell area, M is the carbon atom mass, $f(\epsilon) = 1/[\exp(\frac{\epsilon - E_F}{k_B T}) + 1]$ is the Fermi-Dirac distribution, δ is a broadening factor accounting for charge inhomogeneity, EPC(Γ) is the electron-phonon coupling,[58] s, s' are the band indices, and j, j' are the subband indices. $\phi_{jj'}^{+}$ weighs the EPC contribution for transitions between different subbands in BLG. The values of $\phi_{jj'}^{+}$ are given in Ref. 13 as

$$\phi_{11} = \phi_{22} = 0.5\frac{(\gamma k)^2}{(\gamma_1/2)^2 + (\gamma k)^2},$$

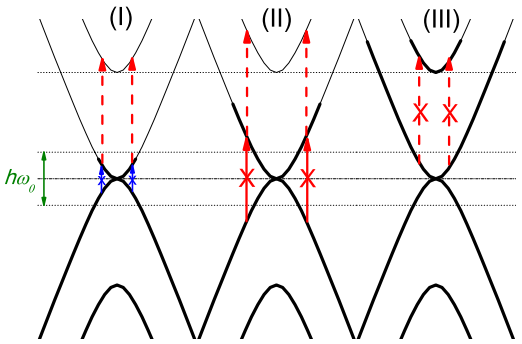

FIG. 7. (Color online) Phonon renormalization for BLG: (i) $E_F<\hbar\omega_0$, (II) $\hbar\omega_0<E_F<\gamma_1$, (III) $E_F>\gamma_1$. Blue (dark gray) and red (light gray) arrows correspond, respectively, to positive and negative contributions to Π. Solid and dashed arrows correspond to interband and intraband processes, respectively.

$$\phi_{12}=\phi_{21}=0.5\frac{(\gamma_1/2)^2}{(\gamma_1/2)^2+(\gamma k)^2}. \tag{14}$$

By using Eqs. (12) and (13) in Eqs. (10) and (11), we get $\Delta\mathrm{Pos}(G)^{\mathrm{dyn}}$ and $\mathrm{FWHM}(G)^{\mathrm{EPC}}$ for SLG and BLG.

To compare Eqs. (10) and (11) to the experimental data, we use $\alpha'=4.4\times10^{-3}$ [obtained from the DFT values of EPC(Γ) [45.6 (eV)^2/Å^2] and v_F (Refs. 21 and 36)], the experimental $\hbar\omega_0$ for SLG and BLG, and $T=300$ K. δ is fitted from the experimental FWHM(G) to FWHM(G) $=\mathrm{FWHM}(G)^{\mathrm{EPC}}+\mathrm{FWHM}(G)^0$, with FWHM($G$)^0 a constant accounting for non-EPC effects (e.g., resolution and anharmonicity). For SLG (BLG) we get $\delta=0.13$ eV (0.03 eV) and FWHM(G)$^0=4.3$ cm^{-1} (5.1 cm^{-1}). These δ values are then used to compute Pos(G). Note that the relation between n and E_F implies that charge inhomogeneity causes different E_F broadening in SLG and BLG (e.g., $\delta n\sim10^{12}$ cm^{-2} would give 0.13 and 0.03 eV in SLG and BLG, respectively).

The solid lines in Fig. 6 are the theoretical Pos(G) and FWHM(G) at 300 K. The experimental and theoretical FWHM(G) are in excellent agreement, as expected since the latter was fitted to the former. The theoretical Pos(G) captures the main experimental features. In particular, the flat dependence for $|E_f|<0.1$ eV in both SLG and BLG and the kink at $\sim$0.4 eV in BLG. This kink is the most striking difference between SLG and BLG. It is the signature of the second subband filling in BLG.

Indeed, a shift of E_F, by acting on $f(\epsilon)$ in Eq. (13), modifies the type and number of transitions contributing to Π. The only transitions giving a positive contribution to Π are those for which $|\epsilon_{s,j,k}-\epsilon_{s',j',k}|<\hbar\omega_0$, i.e., a subset of those between $(s=-1;j=1)$ and $(s=1;j=1)$ [interband transitions, solid blue (dark gray) lines in Fig. 7]. Note that the numerator in Eq. (13) gives a negative value. Interband transitions with $|\epsilon_{s,j,k}-\epsilon_{s',j',k}|>\hbar\omega_0$ [solid red (light gray) lines in Fig. 7] and all intraband [between $(s=\pm1;j=1)$ and $(s=\pm1,j=2)$, dashed red (light gray) lines in Fig. 7] contribute to Π as negative terms. It is convenient to distinguish three different cases: (I) $|E_F|<\hbar\omega_0$, (II) $\hbar\omega_0<|E_F|<\gamma_1$, and (III) $|E_F|>\gamma_1$. For simplicity let us assume $E_F>0$ (the same applies for $E_F<0$). In case (I) the positive contributions from interband transitions are suppressed and new negative intraband transitions are created. This results in strong phonon softening at low temperatures.[41] At $T=300$ K, these effects are blurred by the fractionary occupation of the electronic states, resulting in an almost doping independent phonon energy [see Fig. 6(c)]. In case (II), a shift of E_F suppresses negative interband contributions and creates new negative intraband transitions. By counting their number and relative weight [given by $\Phi_{jj'}/(\epsilon_{s,j,k}-\epsilon_{s',j',k})$], one can show that interband transitions out-weight intraband ones, resulting in phonon hardening. Case (III) is similar to (II), with the difference that the second subband filling suppresses negative intraband transitions at $\mathbf{k}\sim\mathbf{K}$, further enhancing the phonon hardening. Thus, the kink in Fig. 6 is a direct measurement of the interlayer coupling strength from Raman spectroscopy.

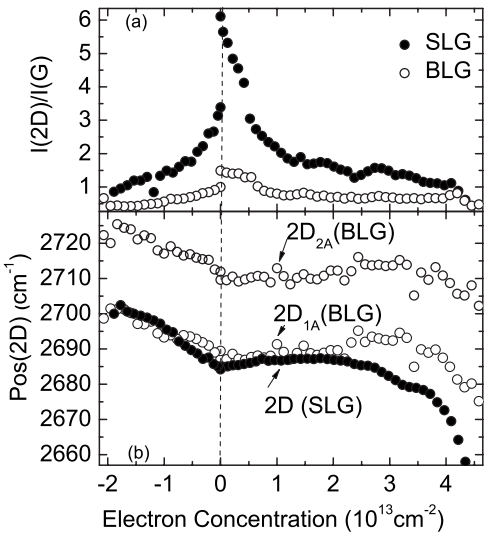

FIG. 8. (a) Ratio of 2D and G peaks intensities for SLG (solid circles) and BLG (open circles) as a function of electron concentration. (b) Position of 2D for SLG (solid circles) and 2D main components for BLG (open circles) as a function of electron concentration.

VI. INTENSITY RATIO

In SLG the intensity ratio of the 2D and G peaks, $I(2D)/I(G)$ has a strong dependence on doping.[25] Figure 8(a) plots $I(2D)/I(G)$ as a function of doping. For BLG we take the highest among $2D_{1A}$ and $2D_{2A}$. The SLG dependence reproduces our previous results.[25] However, we find an almost constant ratio in BLG. Figure 8(b) plots the doping dependence of Pos(2D) in SLG, and Pos($2D_{1A}$), Pos($2D_{2A}$) in BLG. To a first approximation, this is governed by lattice relaxation, which explains the overall stiffening for hole doping and softening for electron doping.[25] A quantitative understanding requires one to consider both EPC and electron-electron interactions.[59] We also note that the shape of the 2D peak changes with doping in BLG. This is due to the relative motion of the four subbands as a result of the relative shift of the conduction and valence bands in BLG when applying a top gate.

VII. CONCLUSIONS

We have simultaneously measured the behavior of optical phonons in single layer and bilayer graphene as a function of doping. In the latter, the *G* peak renormalizes as the Fermi energy moves from the first to the second subband, allowing a direct measurement of $\gamma_1 \sim 0.4$ eV.

ACKNOWLEDGMENTS

We thank D. M. Basko, K. S. Novoselov, and E. McCann for useful discussions. A.K.S. acknowledges funding from the Department of Science and Technology, India, S.P. from Pembroke College and the Maudslay society, and A.C.F. from The Royal Society and the European Research Council project NANOPOTS.

*asood@physics.iisc.ernet.in
†acf26@eng.cam.ac.uk

[1] K. S. Novoselov, A. K. Geim, S. V. Morozov, D. Jiang, Y. Zhang, S. V. Dubonos, I. V. Grigorieva, and A. A. Firsov, Science **306**, 666 (2004).
[2] K. S. Novoselov, A. K. Geim, S. V. Morozov, D. Jiang, M. I. Katsnelson, I. V. Grigorieva, S. V. Dubonos, and A. A. Firsov, Nature (London) **438**, 197 (2005).
[3] Y. Zhang, Y.-W. Tan, H. L. Stormer, and P. Kim, Nature (London) **438**, 201 (2005).
[4] J.-C. Charlier, P. C. Eklund, J. Zhu, and A. C. Ferrari, Top. Appl. Phys. **111**, 673 (2008).
[5] A. K. Geim and K. S. Novoselov, Nature Mater. **6**, 183 (2007).
[6] S. V. Morozov, K. S. Novoselov, M. I. Katsnelson, F. Schedin, D. C. Elias, J. A. Jaszczak, and A. K. Geim, Phys. Rev. Lett. **100**, 016602 (2008).
[7] X. Du, I. Skachko, A. Barker, and E. Y. Andrei, Nat. Nanotechnol. **3**, 491 (2008).
[8] K. I. Bolotin, K. J. Sikes, Z. Jiang, G. Fundenberg, J. Hone, P. Kim, and H. L. Stormer, Solid State Commun. **146**, 351 (2008); K. I. Bolotin, K. J. Sikes, J. Hone, H. L. Stormer, and P. Kim, Phys. Rev. Lett. **101**, 096802 (2008).
[9] M. C. Lemme, T. J. Echtermeyer, M. Baus, and H. Kurz, IEEE Electron Device Lett. **28**, 282 (2007).
[10] M. Y. Han, B. Ozyilmaz, Y. Zhang, and P. Kim, Phys. Rev. Lett. **98**, 206805 (2007).
[11] Z. Chen, Y.-M. Lin, M. J. Rooks, and P. Avouris, Physica E (Amsterdam) **40**, 228 (2007).
[12] E. McCann and V. I. Falko, Phys. Rev. Lett. **96**, 086805 (2006).
[13] T. Ando, J. Phys. Soc. Jpn. **76**, 104711 (2007).
[14] T. Ohta, A. Bostwick, T. Seyller, K. Horn, and E. Rotenberg, Science **313**, 951 (2006).
[15] E. A. Henriksen, Z. Jiang, L.-C. Tung, M. E. Schwartz, M. Takita, Y.-J. Wang, P. Kim, and H. L. Stormer, Phys. Rev. Lett. **100**, 087403 (2008).
[16] E. McCann, Phys. Rev. B **74**, 161403(R) (2006).
[17] E. V. Castro, K. S. Novoselov, S. V. Morozov, N. M. R. Peres, J. M. B. Lopes dos Santos, J. Nilsson, F. Guinea, A. K. Geim, and A. H. Castro Neto, Phys. Rev. Lett. **99**, 216802 (2007).
[18] A. C. Ferrari, J. C. Meyer, V. Scardaci, C. Casiraghi, M. Lazzeri, F. Mauri, S. Piscanec, D. Jiang, K. S. Novoselov, S. Roth, and A. K. Geim, Phys. Rev. Lett. **97**, 187401 (2006).
[19] C. Casiraghi, A. Hartschuh, E. Lidorikis, H. Qian, H. Harutyunyan, T. Gokus, K. S. Novoselov, and A. C. Ferrari, Nano Lett. **7**, 2711 (2007).
[20] P. Blake, E. W. Hill, A. H. Castro Neto, K. S. Novoselov, D. Jiang, R. Yang, T. J. Booth, and A. K. Geim, Appl. Phys. Lett. **91**, 063124 (2007).
[21] S. Pisana, M. Lazzeri, C. Casiraghi, K. S. Novoselov, A. K. Geim, A. C. Ferrari, and F. Mauri, Nature Mater. **6**, 198 (2007).
[22] J. Yan, Y. Zhang, P. Kim, and A. Pinczuk, Phys. Rev. Lett. **98**, 166802 (2007).
[23] C. Casiraghi, S. Pisana, K. S. Novoselov, A. K. Geim, and A. C. Ferrari, Appl. Phys. Lett. **91**, 233108 (2007).
[24] A. C. Ferrari, Solid State Commun. **143**, 47 (2007).
[25] A. Das, S. Pisana, B. Chakraborty, S. Piscanec, S. K. Saha, U. V. Waghmare, K. S. Novoselov, H. R. Krishnamurthy, A. K. Geim, A. C. Ferrari, and A. K. Sood, Nat. Nanotechnol. **3**, 210 (2008).
[26] A. Das, B. Chakraborty, and A. K. Sood, Bull. Mater. Sci. **31**, 579 (2008).
[27] N. Ferralis, R. Maboudian, and C. Carraro, Phys. Rev. Lett. **101**, 156801 (2008).
[28] T. M. G. Mohiuddin, A. Lombardo, R. R. Nair, A. Bonetti, G. Savini, R. Jalil, N. Bonini, D. M. Basko, C. Galiotis, N. Marzari, K. S. Novoselov, A. K. Geim, and A. C. Ferrari, arXiv:0812.1538 (unpublished).
[29] C. Casiraghi, A. Hartschuh, H. Qian, S. Piscanec, C. Georgi, A. Fasoli, K. S. Novoselov, D. M. Basko, and A. C. Ferrari, Nano Lett. **9**, 1433 (2009).
[30] D. C. Elias, R. R. Nair, T. M. G. Mohiuddin, S. V. Morozov, P. Blake, M. P. Halsall, A. C. Ferrari, D. W. Boukhvalov, M. I. Katsnelson, A. K. Geim, and K. S. Novoselov, Science **323**, 610 (2009).
[31] L. M. Malard, J. Nilsson, D. C. Elias, J. C. Brant, F. Plentz, E. S. Alves, A. H. Castro Neto, and M. A. Pimenta, Phys. Rev. B **76**, 201401(R) (2007).
[32] A. C. Ferrari and J. Robertson, Philos. Trans. R. Soc. London, Ser. A **362**, 2267 (2004).
[33] F. Tuinstra and J. L. Koenig, J. Chem. Phys. **53**, 1126 (1970).
[34] A. C. Ferrari and J. Robertson, Phys. Rev. B **61**, 14095 (2000); **64**, 075414 (2001).
[35] C. Thomsen and S. Reich, Phys. Rev. Lett. **85**, 5214 (2000).
[36] S. Piscanec, M. Lazzeri, F. Mauri, A. C. Ferrari, and J. Robertson, Phys. Rev. Lett. **93**, 185503 (2004).
[37] M. Lazzeri and F. Mauri, Phys. Rev. Lett. **97**, 266407 (2006).
[38] M. Lazzeri, S. Piscanec, F. Mauri, A. C. Ferrari, and J. Robertson, Phys. Rev. B **73**, 155426 (2006).
[39] A. Das, A. K. Sood, A. Govindaraj, A. M. Saitta, M. Lazzeri, F. Mauri, and C. N. R. Rao, Phys. Rev. Lett. **99**, 136803 (2007).
[40] T. Ando, J. Phys. Soc. Jpn. **75**, 124701 (2006).
[41] J. Yan, E. A. Henriksen, P. Kim, and A. Pinczuk, Phys. Rev. Lett. **101**, 136804 (2008).
[42] L. M. Malard, D. C. Elias, E. S. Alves, and M. A. Pimenta, Phys. Rev. Lett. **101**, 257401 (2008).

[43] P. R. Wallace, Phys. Rev. **71**, 622 (1947).
[44] J. C. Slonczewski and P. R. Weiss, Phys. Rev. **109**, 272 (1958).
[45] J. W. McClure, Phys. Rev. **108**, 612 (1957).
[46] M. S. Dresselhaus and G. Dresselhaus, Adv. Phys. **51**, 1 (2002).
[47] K. T. Nguyen, A. Gaur, and M. Shim, Phys. Rev. Lett. **98**, 145504 (2007).
[48] C. Lu, Q. Fu, S. Huang, and J. Liu, Nano Lett. **4**, 623 (2004).
[49] J. B. Oostinga, H. B. Heersche, X. Liu, A. F. Morpurgo, and L. M. K. Vandersypen, Nature Mater. **7**, 151 (2008).
[50] Note that in Fig. 3 of Ref. 13 both SLG density of states and electron concentration are multiplied by a factor of 2.
[51] A. H. Castro Neto, F. Guinea, N. M. R. Peres, K. S. Novoselov, and A. K. Geim, Rev. Mod. Phys. **81**, 109 (2009).
[52] L. Pietronero and S. Strassler, Phys. Rev. Lett. **47**, 593 (1981).
[53] W. E. Pickett and P. B. Allen, Phys. Rev. B **16**, 3127 (1977).
[54] P. B. Allen, Phys. Rev. B **6**, 2577 (1972).
[55] Note that the phonon self-energy imaginary part corresponds to the G peak half width at half maximum, HWHM(G), as for Eq. (8) in Ref. 54, thus, the factor 2 to compute FWHM(G) in Eq. (5). This is sometimes neglected in literature. For example, $\Delta\Gamma$ in Eq. (1) of Ref. 22 represents HWHM(G) and not FWHM(G). Reference 22 then compares this to FWHM(G) calculated in Eq. (3) of Ref. 38, finding $D^2/4=\langle D_{\mathbf{\Gamma}}^2\rangle_F$. However, the correct relation should be $D^2/2=\langle D_{\mathbf{\Gamma}}^2\rangle_F$. Because of this, the coupling constant of Ref. 22 is $\lambda=2\alpha'$ instead of $\lambda=\alpha'$. Similarly, "broadening" in Figs. 4 and 6 of Ref. 13 and Fig. 4 of Ref. 40 is HWHM(G) and not FWHM(G). Also, Fig. 6 in Ref. 56 mistakenly compares the experimental FWHM of the G^- peak of metallic single wall carbon nanotubes to the theroetical HWHM.
[56] K. Ishikawa and T. Ando, J. Phys. Soc. Jpn. **75**, 084713 (2006).
[57] Note that the prefactor of Eq. (7) of Ref. 21 should be $\frac{\omega_0\alpha'}{4c}$.
[58] EPC(Γ) is equivalent to $\langle G_{\mathbf{\Gamma}}^2\rangle_F$ as defined in Ref. 38.
[59] D. M. Basko, Phys. Rev. B **78**, 125418 (2008); D. M. Basko, S. Piscanec, and A. C. Ferrari (unpublished).